INTERNATIONAL JOURNAL FOR NUMERICAL METHODS IN FLUIDS, VOL. 14, 217–239 (1992)

HOT FLOW ANALYSIS OF SWIRLING SUDDEN-EXPANSION DUMP COMBUSTOR

SHU-HAO CHUANG

Department of Mechanical Engineering, National Chung-Hsing University, Taichung, Taiwan 40227, R.O.C.

HSUN-CHENG LIN AND FANG-MEI TAI

Shu-Teh Junior College of Technology, Taichung, Taiwan 40202, R.O.C.

AND

HONG-MING SUNG

Graduate School of Mechanical Engineering, Feng-Chia University, Taichung, Taiwan 40724, R.O.C.

SUMMARY

Hot flow of a sudden-expansion dump combustor with swirling is analysed by employing an infinite chemical reaction rate. Turbulence properties are closed using one type of algebraic Reynolds stress model and two types of k–ε model. One of the k–ε models includes a swirling effect modification to the ε-equation. Computations have been performed by the SIMPLE-C algorithm with a power-law scheme. The calculated results of the momentum fields and turbulence quantities for swirling flow are compared with the available experimental data. It is shown that the standard k–ε model gives poor prediction of the mean velocity, particularly the tangential velocity. For the hot flow analysis of a sudden-expansion dump combustor with swirling flow it is suggested that it is necessary to use the modified k–ε model or algebraic Reynolds stress model.

KEY WORDS Swirling flow Swirling angle Combustion flow k–ε model Algebraic Reynolds stress

INTRODUCTION

Good turbulent mixing and high combustion efficiency are the main objectives of successful combustor design. In order to maintain good turbulent mixing and high combustion efficiency, we need to develop recirculation zones in the combustor to prevent the flame of the combustor from being blown out and destabilized. Recirculation zones can be created by the flow of a sudden-expansion dump,[1,2] swirling,[1,3–5] side inlets[6] or flameholders.[7–9]

The flow of a sudden-expansion dump combustor can be characterized[10] by flow separation, flow recirculation, flow reattachment and shear flow. The core flow region and the recirculation flow region are divided by a streamline. The interception point between the dividing steamline and the combustor wall is a reattachment point. The recirculation zone in the corner of a sudden-expansion combustor is called a corner recirculation zone (CRZ) and the recirculation zone on the centreline is called a central toroidal recirculation zone (CTRZ). The recirculation zone is an adverse pressure gradient region. The phenomena of adverse flow and high turbulent

0271–2091/92/020217–23$11.50

Received November 1989
Revised January 1991

fluctuation are created by the adverse pressure gradient. Therefore the turbulent mixing and combustion efficiency benefit when recirculation zones are formed in the combustor.

The properties (e.g. length of reattachment zone, flow stability) of sudden-expansion flow with various Reynolds number were measured by Back and Roschke.[11] The effect of swirling on reacting flow has been analysed by employing a one-step mechanism and the k–ε turbulence model.[3] Two-dimensional axisymmetric combustor flow has been studied by using p–u–v primitive variables and the k–ε turbulence model.[12] The same approach has been used to study the effect of strong swirling on reacting flow.[1,13] The velocity distribution of the sudden-expansion tube was measured by Lu.[2] The prediction of swirling reacting flow in ramjet combustors was investigated by Lilley *et al.*[14] Vatistas *et al.*[7] used the p–u–v method to analyse the axial combustor flow with a bluff-body flameholder. Numerical simulation of the diffusion flame of an afterburner with V-gutter flameholders has been carried out by employing the SIMPLE-C algorithm and the k–ε turbulence model.[9,15] Swirling flow promotes the combustion efficiency of a combustor[16] (e.g. a gas turbine or a furnace) by enhancing turbulent mixing and increases the stability of the flame via the action of recirculation. For strongly swirling flow the fully elliptic character of the recirculation causes axial flow reversal at the centreline and there is no dominant flow direction. For this reason the standard k–ε model seems to give unsatisfactory predicted computations for swirling jet flow.[17,18] The poor predicted computations have been attributed to the inappropriate assumption of an isotropic eddy viscosity and to the commonly used form of the ε-equation not being suitable for flow with swirling.[19] A number of computational studies support this result that the standard model with isotropic eddy viscosity and no extra swirling-related terms yields poor predictions for strongly swirling jets.[20,21] To rectify these problems, we have made a swirling-related modification to the ε-equation and compared the results for this modified equation with those of the standard k–ε model. Agreement with experimental data is achieved through Richardson number corrections.[1,12,21–23] For the non-isotropic eddy viscosity we have used an algebraic Reynolds stress model[24] which is a direct approximation of the Reynolds stress equation, retaining its anisotropy.[19] Computations with the standard and swirling-corrected k–ε models and the algebraic Reynolds stress model are presented for the effect of swirling on the reacting flow of a sudden-expansion dump combustor.

THEORETICAL MODEL

In order to simplify the problem and thus facilitate the numerical simulation, we make the following assumptions.

1. Density fluctuations and gravity effects are not considered.
2. The flow is axisymmetric and steady state.
3. The wall thickness of a V-gutter is infinitely thin.
4. The Lewis number is equal to unity and the specific heat at constant pressure is a constant.
5. The chemical (one-step) reaction rate is infinitely fast.

The governing equation for the axisymmetric flow is of the elliptic type. The general form of the Favre-averaged equation for steady axisymmetric flow can be written as[1]

$$\frac{1}{r}\left[\underbrace{\frac{\partial}{\partial x}(r\rho U\phi)+\frac{\partial}{\partial r}(r\rho V\phi)}_{\text{convection}}-\underbrace{\frac{\partial}{\partial x}\left(r\Gamma_\phi\frac{\partial\phi}{\partial x}\right)-\frac{\partial}{\partial r}\left(r\Gamma_\phi\frac{\partial\phi}{\partial r}\right)}_{\text{diffusion}}\right]=\underbrace{S^\phi}_{\text{source}}. \tag{1}$$

The physical quantities for ϕ and Γ_ϕ are listed in Table I.

Table I. Governing equation variables

ϕ	Γ_ϕ	S^ϕ	$S_p/\Delta V$	$S_c/\Delta V$
U	μ_e	$-\frac{\partial P}{\partial x}+S^u$	0	$S^u-\frac{\partial P}{\partial r}$
V	μ_e	$-\frac{\partial P}{\partial r}-\frac{2\mu_e V}{r^2}+\frac{\rho W^2}{r}+S^v$	$-\frac{2\mu_e}{r^2}$	$S^v-\frac{\partial P}{\partial r}+\frac{\rho W^2}{r}$
W	μ_e	$-\frac{\rho VW}{r}-\frac{W}{r^2}\frac{\partial}{\partial r}(r\mu_e)$	0	S^w
k	$\frac{\mu_e}{\sigma_k}$	$G-\rho\varepsilon$	$-\frac{C_\mu\rho^2 k}{\mu_e}$	G
ε	$\frac{\mu_e}{\sigma_\varepsilon}$	$\frac{C_1\varepsilon G-C_2\rho\varepsilon^2}{k}$	$-\frac{C_2\rho\varepsilon}{k}$	$\frac{C_1 G\varepsilon}{k}$

$$S^u=\frac{\partial}{\partial x}\left(\mu_e\frac{\partial U}{\partial x}\right)+\frac{1}{r}\frac{\partial}{\partial r}\left(r\mu_e\frac{\partial V}{\partial x}\right)-\frac{2}{3}\frac{\partial}{\partial x}\left[\frac{\mu_e}{r}\left(\frac{\partial}{\partial x}(rU)+\frac{\partial}{\partial r}(rV)\right)+\rho k\right]$$

$$S^v=\frac{\partial}{\partial x}\left(\mu_e\frac{\partial U}{\partial r}\right)+\frac{1}{r}\frac{\partial}{\partial r}\left(r\mu_e\frac{\partial V}{\partial r}\right)-\frac{2}{3}\frac{\partial}{\partial r}\left[\frac{\mu_e}{r}\left(\frac{\partial}{\partial x}(rU)+\frac{\partial}{\partial r}(rV)\right)+\rho k\right]$$

$$S^w=-\frac{\rho VW}{r}-\frac{W}{r^2}\frac{\partial}{\partial r}(r\mu_e)$$

$$G=\mu_e\left\{2\left[\left(\frac{\partial U}{\partial x}\right)^2+\left(\frac{\partial V}{\partial r}\right)^2+\left(\frac{V}{r}\right)^2\right]+\left(\frac{\partial U}{\partial r}+\frac{\partial V}{\partial x}\right)^2+\left[r\frac{\partial}{\partial x}\left(\frac{W}{r}\right)^2\right]+\left(\frac{\partial W}{\partial x}\right)^2\right\}$$

Reynolds stress equation for a swirling flow in modelled form

For the swirling flow problem our starting point for the derivation of the transport equations of Reynolds stresses is the Navier–Stokes equations, which can be expressed as

$$\underbrace{(\mathbf{v}\cdot\nabla)\mathbf{v}}_{\text{I}}=\underbrace{-(1/\rho)\nabla p}_{\text{II}}+\underbrace{\nu\nabla^2\mathbf{v}}_{\text{III}}. \tag{2}$$

The double-correlation equations for $\overline{u_i u_j}$ are derived from equation (2). For turbulence at high Reynolds number, viscous diffusion is negligible and the small-scale motion is isotropic. Secondary generation terms given by Launder and Morse[25] are discarded here for simplification. The double correlations in axisymmetric swirling flow may be written as[26]

$$U\frac{\partial\bar{u}^2}{\partial x}+V\frac{\partial\bar{u}^2}{\partial r}=-\frac{1}{r}\frac{\partial}{\partial r}(r\overline{vu^2})-2\overline{vu}\frac{\partial U}{\partial r}+2\overline{\frac{p}{\rho}\frac{\partial u}{\partial x}}-\tfrac{2}{3}\varepsilon, \tag{3}$$

$$U\frac{\partial\bar{v}^2}{\partial x}+V\frac{\partial\bar{v}^2}{\partial r}-2\overline{vw}\frac{W}{r}=-\frac{1}{r}\frac{\partial}{\partial r}\left(r\bar{v}^3+2r\overline{\frac{pv}{\rho}}\right)+2\frac{\overline{vw}^2}{r}+2\overline{vw}\frac{W}{r}+\frac{2}{r}\overline{\frac{p}{\rho}\frac{\partial}{\partial r}(rv)}-\tfrac{2}{3}\varepsilon, \tag{4}$$

$$U\frac{\partial\bar{w}^2}{\partial x}+V\frac{\partial\bar{w}^2}{\partial r}+2\overline{vw}\frac{W}{r}=-\frac{1}{r}\frac{\partial}{\partial r}(r\overline{vw}^2)-2\frac{\overline{vw}^2}{r}-2\overline{vw}\frac{\partial W}{\partial r}-\tfrac{2}{3}\varepsilon, \tag{5}$$

$$U\frac{\partial\overline{uv}}{\partial x}+V\frac{\partial\overline{uv}}{\partial r}-\overline{uw}\frac{W}{r}=-\frac{1}{r}\frac{\partial}{\partial r}\left(r\overline{uv^2}+r\frac{\overline{pu}}{\rho}\right)-\bar{v}^2\frac{\partial U}{\partial r}+\overline{uw}\frac{W}{r}+\overline{\frac{p}{\rho}\left(\frac{\partial u}{\partial x}+\frac{1}{r}\frac{\partial}{\partial r}(rv)\right)}, \tag{6}$$

$$U\frac{\partial\overline{uw}}{\partial x}+V\frac{\partial\overline{uw}}{\partial r}+\overline{uv}\frac{W}{r}=-\frac{1}{r}\frac{\partial}{\partial r}(r\overline{uvw})-\frac{\overline{uvw}}{r}-\overline{vw}\frac{\partial W}{\partial r}+\overline{\frac{p}{\rho}\frac{\partial u}{\partial x}}, \tag{7}$$

$$U\frac{\partial\overline{vw}}{\partial x}+V\frac{\partial\overline{vw}}{\partial r}+(\bar{v}^2-\bar{w}^2)\frac{W}{r}=-\frac{1}{r}\frac{\partial}{\partial r}\left(r\overline{wv^2}+r\frac{\overline{pw}}{\rho}\right)-\frac{\overline{wv^2}}{r}+\frac{\bar{w}^3}{r}-\bar{v}^2\frac{\partial W}{\partial r}+\bar{w}^2\frac{W}{r}+\frac{\bar{p}}{r\rho}\frac{\overline{\partial(rv)}}{\partial r}. \tag{8}$$

The pressure–strain correlations consist of two components, one the mutual interaction of the fluctuating velocities and the other the interaction of the mean rate of strain with the turbulence. Rotta's proposal[27] is generally used to model the first term. Some suggestions have been made for modelling the second term.[27–29] Here we choose to adopt the Naot *et al.*[29] formulation because of its simplicity. Therefore the pressure–strain correlations can be modelled as[29]

$$ps_{ij}=\underbrace{\frac{C_1\varepsilon}{k(\overline{u_iu_j}-\frac{2}{3}k\delta_{ij})}}_{\text{due to Rotta}^{27}}-\underbrace{C_2(P_{ij}-\tfrac{2}{3}P_{ij}\delta_{ij})}_{\text{due to Naot } et\ al.^{29}}, \tag{9}$$

where P_{ij} are the production terms and P_k is the production of turbulence kinetic energy. The differential character of equations (3)–(8) can be eliminated by the modelled form of Rodi[30] that the convection less the diffusion of a Reynolds stress is proportional to the convection less the diffusion of the turbulence kinetic energy k in the ratio of the value of the Reynolds stress to the value of the turbulence kinetic energy.

The algebraic Reynolds stress equations are given when we substitute the expressions of equation (9) into equations (3)–(8)

$$\overline{u_iu_j}=\frac{k}{P_k+\varepsilon(C_1-1)}\{\tfrac{2}{3}\delta_{ij}[C_2P_k+\varepsilon(C_1-1)]+P_{ij}(1-C_2)\}. \tag{10}$$

Six Reynolds stresses can be obtained from equation (10). The stress production terms P_{ij} are the corresponding ones of equations (3)–(8). Consequently, closure of the set of stress equations requires only the additional production turbulence energy P_k and turbulence dissipation rate ε. The turbulence kinetic energy k-equation and turbulence dissipation rate ε-equation can be constructed from Table I.

$$\underbrace{\frac{\partial(Uk)}{\partial x}+\frac{1}{r}\frac{\partial(rVk)}{\partial r}}_{\text{convection}}=\underbrace{\frac{\partial}{\partial x}\left(\frac{\nu_t}{\sigma_k}\frac{\partial k}{\partial x}\right)+\frac{1}{r}\frac{\partial}{\partial r}\left(\frac{r\nu_t}{\sigma_k}\frac{\partial k}{\partial r}\right)}_{\text{diffusion}}\underbrace{+G}_{\text{production}}\underbrace{-\varepsilon}_{\text{dissipation}}, \tag{11}$$

where

$$G=\nu_t\left\{2\left[\left(\frac{\partial U}{\partial x}\right)^2+\left(\frac{\partial V}{\partial r}\right)^2+\left(\frac{V}{r}\right)^2\right]+\left(\frac{\partial U}{\partial r}+\frac{\partial V}{\partial x}\right)^2+\left(\frac{\partial W}{\partial x}\right)^2+\left[r\frac{\partial}{\partial r}\left(\frac{W}{r}\right)^2\right]\right\},$$

and

$$\underbrace{\frac{\partial(U\varepsilon)}{\partial x}+\frac{1}{r}\frac{\partial(rV\varepsilon)}{\partial r}}_{\text{convection}}=\underbrace{\frac{\partial}{\partial x}\left(\frac{\nu_t}{\sigma_\varepsilon}\frac{\partial\varepsilon}{\partial x}\right)+\frac{1}{r}\frac{\partial}{\partial r}\left(\frac{r\nu_t}{\sigma_\varepsilon}\frac{\partial\varepsilon}{\partial r}\right)}_{\text{diffusion}}+\underbrace{\frac{\varepsilon}{k}(C_1G}_{\text{production}}\underbrace{-C_2f\varepsilon)}_{\text{dissipation}}, \tag{12}$$

where the correction of the ε-equation is expressed as a function f multiplying C_2 and the empirical constants are $C_\mu = 0{\cdot}09$, $\sigma_k = 1$, $\sigma_\varepsilon = 1{\cdot}22$, $C_1 = 1{\cdot}44$ and $C_2 = 1{\cdot}92$. The function f is given by[31,32]

$$f = 1 - 0{\cdot}2Ri, \tag{13}$$

where Ri is a gradient Richardson number defined by

$$Ri = \frac{k^2}{\varepsilon^2}\frac{W}{r^2}\frac{\partial(rW)}{\partial r}. \tag{14}$$

Turbulence model

The total effective viscosity μ_e of the flow is

$$\mu_e = \mu_l + \mu_t \tag{15}$$

where μ_l and μ_t represent the molecular and eddy viscosity respectively and μ_t is known from the k–ε turbulence model[33] as

$$\mu_t = C_\mu \rho k^2/\varepsilon. \tag{16}$$

Combustion model

In the present analysis CH_4 is used as the fuel and thus the chemical reaction equation can be written as

$$CH_4 + 2(O_2 + 3{\cdot}76N_2) \xrightarrow{\omega} CO_2 + 2H_2O + 7{\cdot}52N_2 + \Delta H \tag{17a}$$

or

$$(1\text{ kg})\text{ fuel} + (s\text{ kg})\text{ oxidant} + (a\text{ kg})\,N_2 \xrightarrow{\omega} [(1+s)\text{kg}]\text{ products} + (a\text{ kg})\,N_2 + \Delta H. \tag{17b}$$

The species conservation equations of fuel and oxidant are

$$\frac{\partial}{\partial x}(\rho U m_{fu}) + \frac{1}{r}\frac{\partial}{\partial r}(r\rho V m_{fu}) - \frac{\partial}{\partial x}\left(\frac{\mu_e}{\sigma_{fu}}\frac{\partial m_{fu}}{\partial x}\right) - \frac{1}{r}\frac{\partial}{\partial r}\left(r\frac{\mu_e}{\sigma_{fu}}\frac{\partial m_{fu}}{\partial r}\right) = m'_{fu}, \tag{18}$$

$$\frac{\partial}{\partial x}(\rho U m_{ox}) + \frac{1}{r}\frac{\partial}{\partial r}(r\rho V m_{ox}) - \frac{\partial}{\partial x}\left(\frac{\mu_e}{\sigma_{ox}}\frac{\partial m_{ox}}{\partial x}\right) - \frac{1}{r}\frac{\partial}{\partial r}\left(r\frac{\mu_e}{\sigma_{ox}}\frac{\partial m_{ox}}{\partial r}\right) = m'_{ox}, \tag{19}$$

Subtracting equation (18) multiplied by s from equation (19), we can obtain the species equation for the modified mass fraction m_{fo} as

$$\frac{\partial}{\partial x}(\rho U m_{fo}) + \frac{1}{r}\frac{\partial}{\partial r}(r\rho V m_{fo}) - \frac{\partial}{\partial x}\left(\frac{\mu_e}{\sigma_{fo}}\frac{\partial m_{fo}}{\partial x}\right) - \frac{1}{r}\frac{\partial}{\partial r}\left(r\frac{\mu_e}{\sigma_{fo}}\frac{\partial m_{fo}}{\partial r}\right) = 0, \tag{20}$$

where

$$m_{fo} = m_{ox} - s m_{fu},$$

and the energy equation is

$$\frac{\partial}{\partial x}(\rho U E) + \frac{1}{r}\frac{\partial}{\partial r}(r\rho V E) - \frac{\partial}{\partial x}\left(\frac{\mu_e}{\sigma_e}\frac{\partial E}{\partial x}\right) - \frac{1}{r}\frac{\partial}{\partial r}\left(r\frac{\mu_e}{\sigma_e}\frac{\partial E}{\partial r}\right) = -m'_{fu}\Delta H, \tag{21}$$

where

$$E = C_p T + \tfrac{1}{2}(U^2 + V^2 + W^2).$$

Adding equation (18) multiplied by ΔH to equation (21), we can obtain the equation for the total

enthalpy F as

$$\frac{\partial}{\partial x}(\rho UF)+\frac{1}{r}\frac{\partial}{\partial r}(\rho rVF)-\frac{\partial}{\partial x}\left(\frac{\mu_e}{\sigma_f}\frac{\partial F}{\partial x}\right)-\frac{1}{r}\frac{\partial}{\partial r}\left(r\frac{\mu_e}{\sigma_f}\frac{\partial F}{\partial r}\right)=0, \tag{22}$$

where

$$F=E+m_{fu}\Delta H=C_pT+\tfrac{1}{2}(U^2+V^2+W^2)+m_{fu}\Delta H$$

According to assumption 5, the infinitely fast chemical reaction rate (i.e. $\omega\to\infty$) implies that fuel and oxidant will not coexist at the same time. Therefore the following relations exist in the flow:

$$m_{fu}+m_{ox}+m_{pr}=1,$$

$$m_{fu}=m_{fo} \quad \text{and} \quad m_{ox}=0 \qquad \text{when } m_{fo}=0,$$

$$m_{fu}=0 \quad \text{and} \quad m_{ox}=m_{fo} \qquad \text{when } m_{fo}>0,$$

$$m_{ox}=0 \quad \text{and} \quad m_{fu}=-(1/s)m_{fo} \qquad \text{when } m_{fo}<0.$$

Boundary conditions

1. At the inlet:
   (a) axial velocity assumed uniform (i.e. $U_{in}=$constant)
   (b) radial velocity $V_{in}=0$
   (c) tangential velocity $W_{in}=U_{in}\tan\theta$
   (d) the turbulence energy and dissipation rate can be written as[34]

$$k_{in}=0{\cdot}003\,U_{in}^2, \qquad \varepsilon_{in}=\frac{C_\mu k_{in}^{3/2}}{0{\cdot}03R},$$

   where R is the radius of the combustor

   (e)

$$m_{fo}=1, \quad m_{fu}=0 \quad \text{and} \quad m_{ox}=1 \quad \text{in the region of the air inlet,}$$

$$m_{fo}=-s, \quad m_{fu}=1 \quad \text{and} \quad m_{ox}=0 \quad \text{in the region of fuel injection.}$$

2. On the centreline:

$$\frac{\partial\Phi}{\partial r}=0 \quad \text{(due to symmetry)}, \qquad V=0, \qquad W=0.$$

3. At the wall: $U=0$, $V=0$ and $W=0$ (no-slip condition). Both k and ε are handled by the wall function.[33,35]
4. At the outlet. The length of fully developed flow for the sudden-expansion dump combustor is normally about $4D$.[12] In the present analysis the length of fully developed flow is $L=6D$ for dump combustor flow with a V-gutter:

$$\frac{\partial\Phi}{\partial x}=0 \quad \text{(fully developed flow)}, \qquad V=0.$$

NUMERICAL ANALYSIS

Grid system

The numerical calculation domain and grid used here are shown in Figure 1. The upstream boundary is 0·325D from the sudden-expansion section so that the boundary condition will not appreciably affect the flow region of the sudden expansion. The grid size contracts in the radial direction and expands in the axial direction from the sudden expansion towards downstream; hence a finer grid spacing is formed near the combustor wall and the vertical wall at the sudden expansion respctively. In the present computation domain a 58×31 grid system with 0·95 contraction in the radial direction and 1·05 expansion in the axial direction is employed. The central processor time on a CDC Cyber 180/830 computer is about 6 h to convergence for 300 iterations per case. The convergence conditions are local residual less than or equal to 10^{-6} and total residual less than or equal to 10^{-4}. The residual of any variable is defined as

$$R_{\mathrm{p}}^{\phi} = a_{\mathrm{p}}\phi_{\mathrm{p}} - \sum_{i=\mathrm{n,s,w,e}} |a_i\phi_i - S^{\phi}|.$$

Finite difference equations

Integration over the control volume cell and the SIMPLE-C algorithm along with a power-law scheme are employed to perform the calculations. The general forms of the finite difference equations for equation (1) with linearized source term are given as follows.

Finite difference equation of the axial momentum:

$$(a_{\mathrm{e}} - S_{\mathrm{p}}^{u})u_{\mathrm{e}} = \Sigma a_{\mathrm{nb}}u_{\mathrm{nb}} + b^{u} + A_{\mathrm{e}}(P_{\mathrm{p}} - P_{\mathrm{e}}), \tag{23}$$

where

$$b^{u} = S_{\mathrm{c}}^{u}\Delta V.$$

Finite difference equation of the radial momentum:

$$(a_{\mathrm{e}} - S_{\mathrm{p}}^{v})u_{\mathrm{e}} = \Sigma a_{\mathrm{nb}}u_{\mathrm{nb}} + b^{v} + A_{\mathrm{e}}(P_{\mathrm{p}} - P_{\mathrm{n}}), \tag{24}$$

where

$$b^{v} = S_{\mathrm{c}}^{v}\Delta V.$$

Finite difference equation of the other variables:

$$(a_{\mathrm{p}} - S_{\mathrm{p}}^{\phi})\phi_{\mathrm{p}} = \Sigma a_{\mathrm{nb}}\phi_{\mathrm{nb}} + b^{\phi}, \tag{25}$$

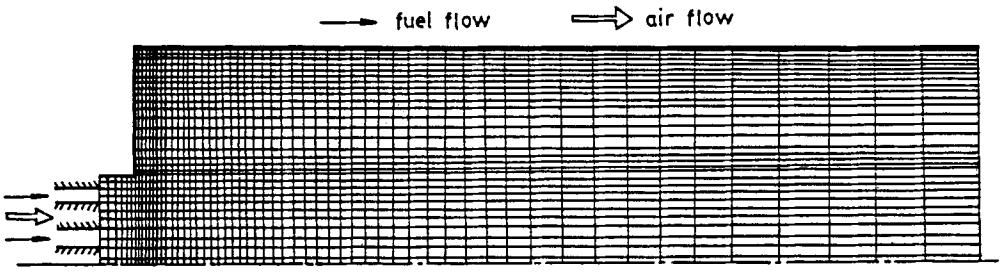

Figure 1. Grid system

where

$$b^{\phi} = S_c^{\phi} \Delta V.$$

The linearized source terms S_c and S_p are listed in Table I.

Solution process

The SIMPLE-C algorithm[9,15] and power-law scheme are employed to calculate the present analysis. The TDMA and line-by-line methods are used to sweep alternately in the x- and r-directions. Underrelaxation factors are used for each iteration process to help the convergence of the calculations. The values of the underrelaxation factors are listed in Table II.

RESULTS AND DISCUSSION

In order to compare our calculated results with the experimental data of Chaturvedi[36] and Lilley,[31] the simulation conditions for the present problem are listed in Table III. The geometry of the sudden-expansion dump combustor configuration is shown in Figure 2.

The reattachment length of the corner recirculation zone (CRZ) of the dump combustor for various swirling angles is shown in Figure 3. The present calculations are in good agreement with the experimental data of Chaturvedi[36] and Lilley.[31] The axial velocity distributions for 58×31 grid points at $X/D = 1$ and 3 for the dump combustor without the swirling effect are compared with the experimental data of Lilley[31] in Figures 4 and 5 and show very good agreement. The axial velocity distributions for 52×22 grid points are also shown in Figures 4 and 5. The calculated results deviate from the experimental data in this case, particularly in the region between the wall and the centre, owing to the diffusion error of grid points with large grid size. The 58×31 grid is utilized for the following analyses. Figure 6 shows the results for the axial velocity ($\theta = 45°$) obtained by using the standard k–ε, the k–ε–R; and the algebric Reynolds stress (ARS) turbulence models, compared with the experimental data of Lilley.[31] As can be seen, the

Table II. Underrelaxation factors f

Without	ϕ	U	V	W	k	ε	m_{fo}	F	p	ρ	μ_t
flameholder	f	0·2	0·2	0·1	0·3	0·5	0·8	0·8	0·3	0·1	0·3
With	ϕ	U	V	W	k	ε	m_{fo}	F	p	ρ	μ_t
flameholder	f	0·2	0·2	0·2	0·5	0·5	0·8	0·8	0·3	0·1	0·3

Table III. Simulation conditions of sudden-expansion dump combustor

Length of combustor	$L = 0{\cdot}5\,\text{m}$
Diameter of combustor	$D = 0{\cdot}125\,\text{m}$
Inlet diameter of combustor	$D_0 = 0{\cdot}0625\,\text{m}$
Expansion ratio	$D/D_0 = 2$
Reynolds number	$Re = 1{\cdot}26 \times 10^5$
Density of air	$\rho = 1{\cdot}2111\,\text{kg m}^{-3}$
Dynamic viscosity of air	$\mu = 1{\cdot}8 \times 10^{-5}\,\text{kg m}^{-1}\,\text{s}^{-1}$

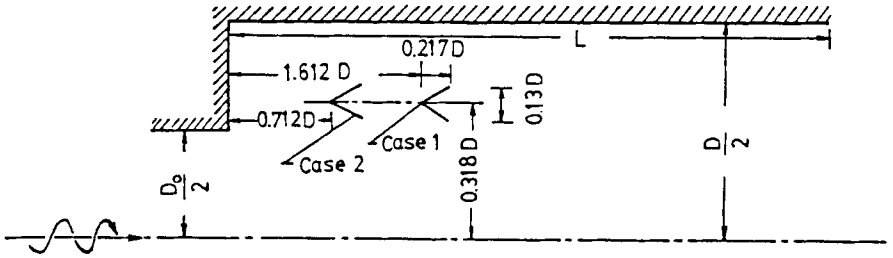

Figure 2. Basic configuration of sudden-expansion dump combustor

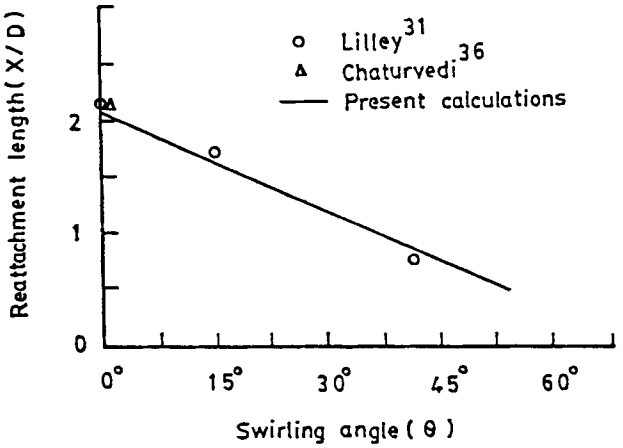

Figure 3. Reattachment length of dump combustor for various swirling angles

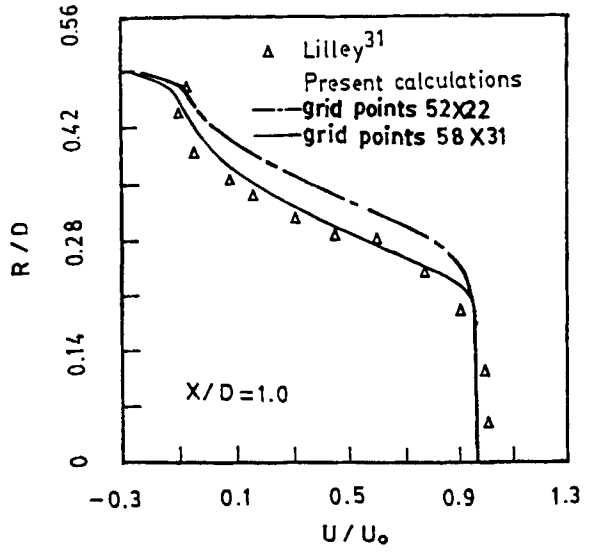

Figure 4. Axial velocity distribution of dump combustor ($\theta = 0°$, $X/D = 1$)

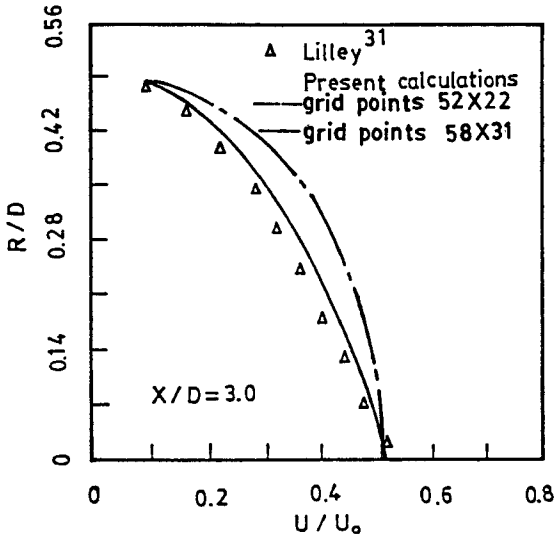

Figure 5. Axial velocity distribution of dump combustor ($\theta = 0°$, $X/D = 3$)

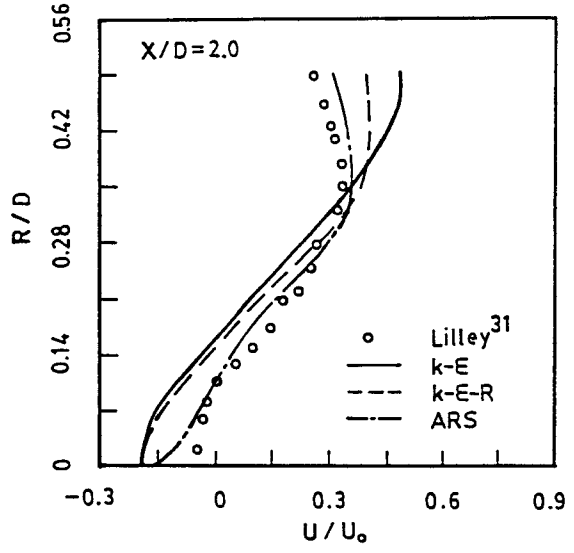

Figure 6. Axial velocity distribution ($\theta = 45°$)

standard k–ε model gives a bad prediction, in particular around the centreline. The overprediction of the standard k–ε model for the cross-section $X/D = 2$ as shown in Figure 6 is largely due to the destabilization effect of swirling on the length scale of the turbulent eddies. Comparing the calculated results between the k–ε and k–ε–R models, the latter gives the better prediction. The improvement with the k–ε–R model is based on the stabilization of the swirling effect through the increasing length scale of turbulent eddies. Equation (13) essentially determines the stabilizing

or destabilizing effect of a radial force on the lateral turbulent fluctuations.[32] The correction of equation (13) predicts a turbulence-damping effect over large regions ($0° < \theta < 70°$) of swirling dump combustor flow where $\partial(rw)/\partial r$ is positive, leading to a reduction in the eddy viscosity. The model gives a better prediction than the other two models since it can predict the anisotropic eddy viscosities, e.g. in the near-wall region for $X/D = 2$, as shown in Figure 6. Figure 7 shows that the swirling effect reduces the centreline tangential velocity ($\theta = 45°$). Although the Richardson

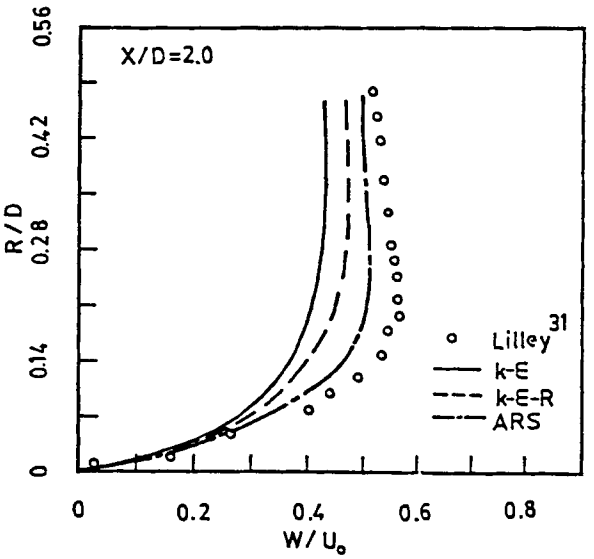

Figure 7. Tangential velocity distribution ($\theta = 45°$)

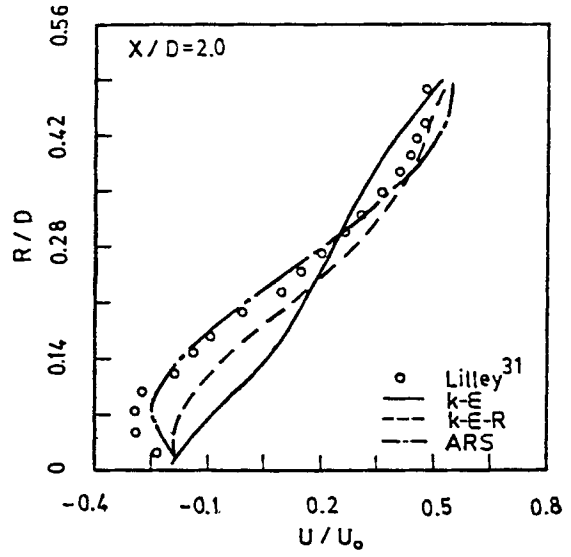

Figure 8. Axial velocity distribution ($\theta = 70°$)

correction factor improves the axial velocity, it has little influence on the tangential velocity. Figure 8 shows the axial velocity distribution for strongly swirling flow ($\theta = 70°$). The ARS model still gives a better prediction than the other two models when compared with the experimental data of Lilley,[31] as shown in Figures 7 and 8.

The turbulent kinetic energy contour of the sudden-expansion dump combustor without swirling is shown in Figure 9. The region of high turbulent kinetic energy is located at the corner, where a recirculation zone has formed. The turbulent kinetic energy contour for a swirling angle of 70° is shown in Figure 10. The region of high turbulent kinetic energy in this case is located in the central toroidal recirculation zone as a result of the swirling effect. The turbulent kinetic energy distributions for axial cross-sections at various swirling angles are shown in Figures 11 and 12. For the cross-section $0{\cdot}393X/D$ the maximum turbulent kinetic energies for $\theta = 60°$ and 70° are located at $0{\cdot}08Y/D$ and $0{\cdot}165Y/D$ respectively. The turbulent kinetic energy for $1{\cdot}356X/D$ tends to be fully developed and the turbulent kinetic energy is larger when the inlet swirling angle is increased. The effects of the V-gutter flameholder configuration on the turbulent kinetic energy of the combustor without swirling are shown in Figures 13 and 14. The region of high turbulent energy appears at the back of the V-gutter flameholder. The effects of the V-gutter configuration on the turbulent energy of the combustor at a swirling angle of 70° are shown in Figures 15 and 16. The maximum turbulent energy of the combustor approaches the centreline owing to the strong swirling effect.

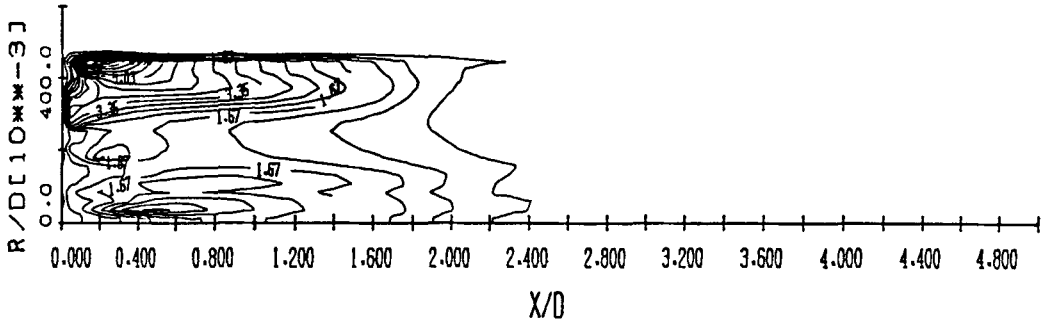

Figure 9. Turbulent kinetic energy contour ($\theta = 0°$, without flameholder)

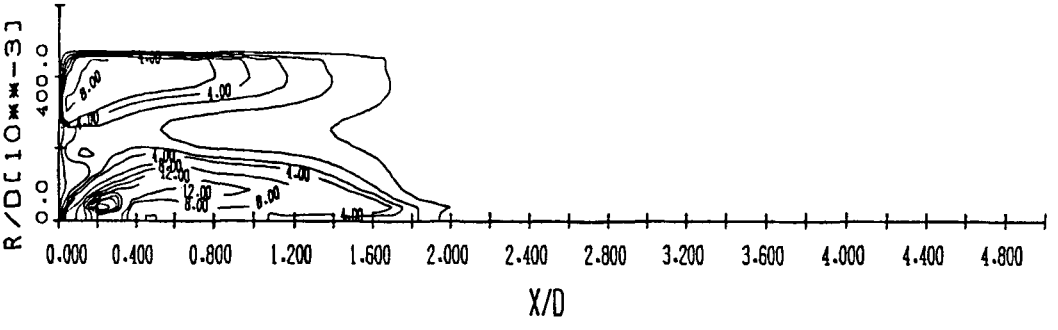

Figure 10. Turbulent kinetic energy contour ($\theta = 70°$, without fllameholder)

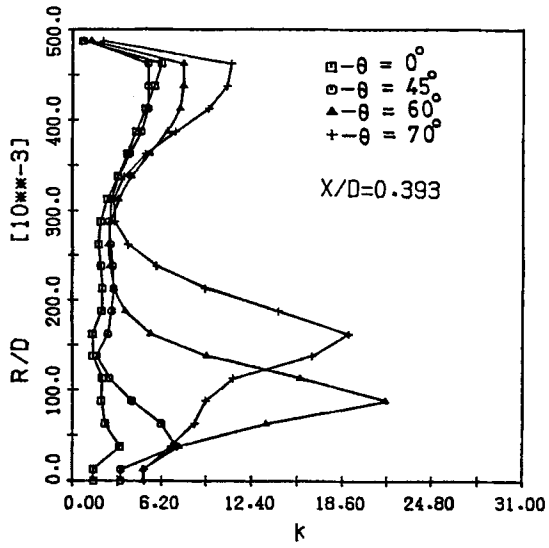

Figure 11. Turbulent kinetic energy distribution at $X/D = 0{\cdot}393$ for various swirling angles (without flameholder)

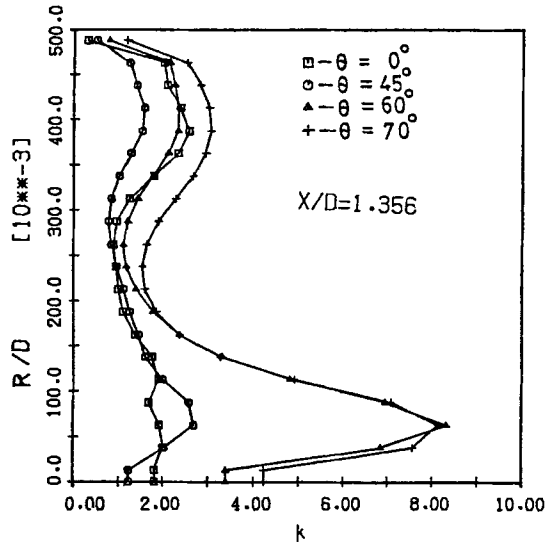

Figure 12. Turbulent kinetic energy distrubition at $X/D = 1{\cdot}356$ for various swirling angles (without flameholder)

The combustion model of the present analysis is a diffusion flame type. Therefore high temperatures occur at the diffusion surface between air and fuel as shown in Figure 17. The temperature distribution for $\theta = 45°$ is shown in Figure 18. The temperature at the inlet is low because the combustion process is incomplete in this region. The fuel in the central toroidal recirculation zone has achieved complete mixing after the cross-section $1{\cdot}356X/D$. Hence the temperature of the central toroidal recirculation zone reaches as high as 2200 K. The temper-

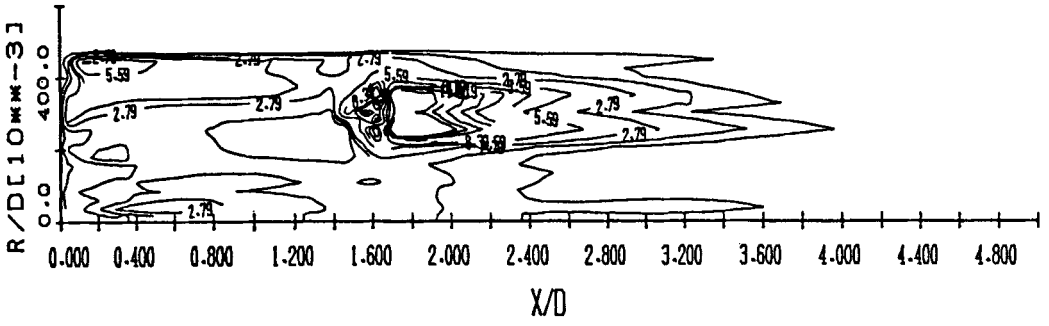

Figure 13. Turbulent kinetic energy contour for case 1 ($\theta = 0°$)

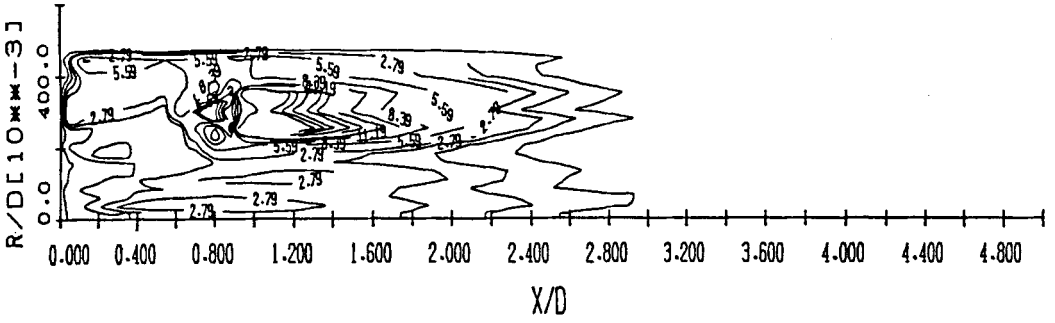

Figure 14. Turbulent kinetic energy contour for case 2 ($\theta = 0°$)

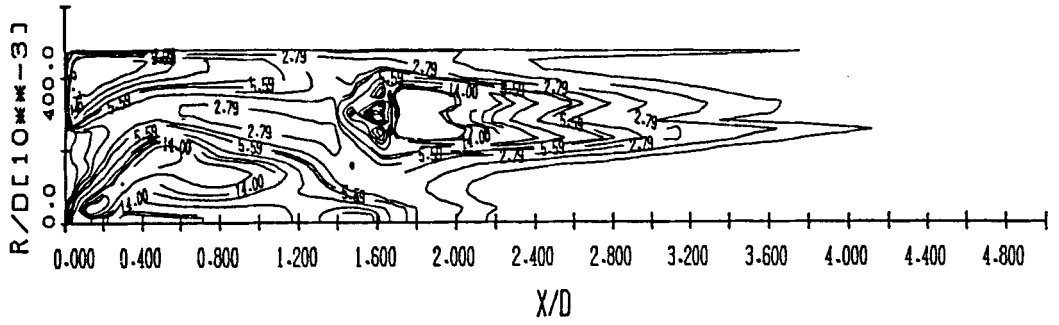

Figure 15. Turbulent kinetic energy contour for case 1 ($\theta = 70°$)

ature distribution for $\theta = 70°$ is shown in Figure 19. The temperature at the inlet reaches about 2200 K because the high-temperature products downstream are driven upstream by the swirling effect and good pre-heated action. The temperature distributions at the cross-section $X/D = 1{\cdot}356$ for various inlet swirling angles are shown in Figure 20. The temperature is increased for larger inlet swirling angle owing to the swirling effect. The effects of the V-gutter flameholder configuration on the temperature distribution without swirling are shown in Figures 21 and 22. The

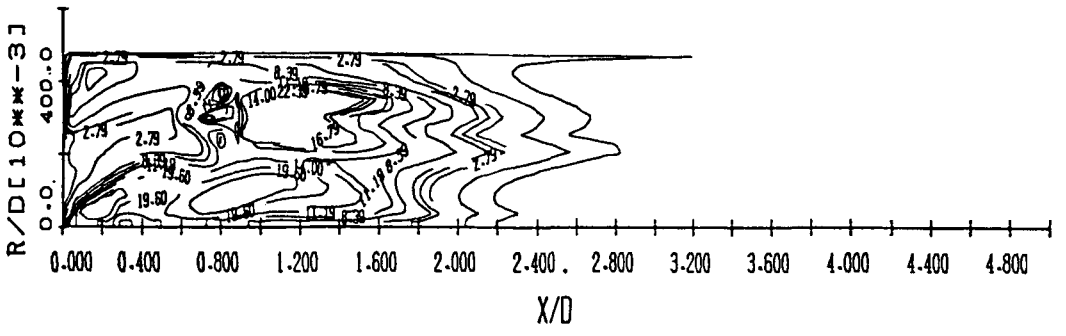

Figure 16. Turbulent kinetic energy contour for case 2 ($\theta = 70°$)

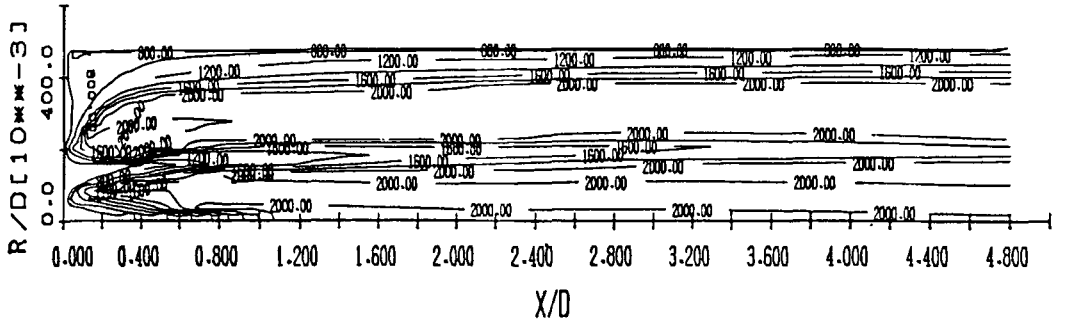

Figure 17. Temperature contours ($\theta = 0°$, without flameholder)

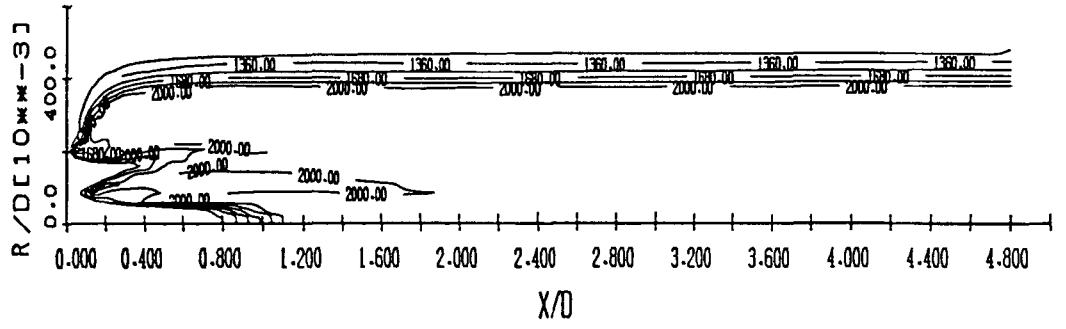

Figure 18. Temperature contours ($\theta = 45°$, without flameholder)

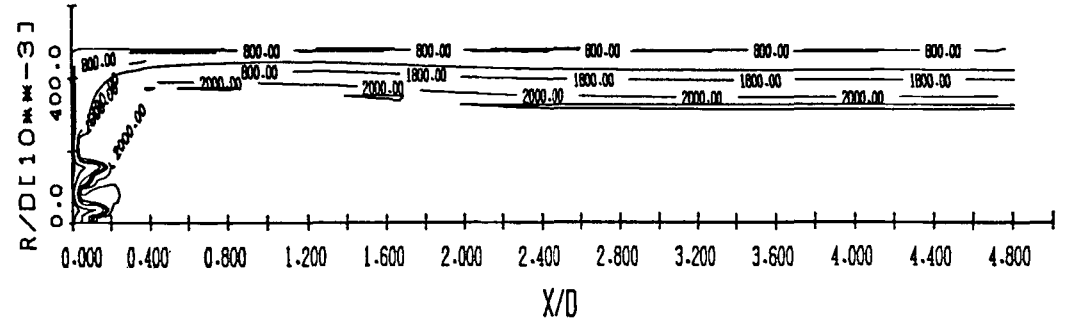

Figure 19. Temperature contours ($\theta = 70°$, without flameholder)

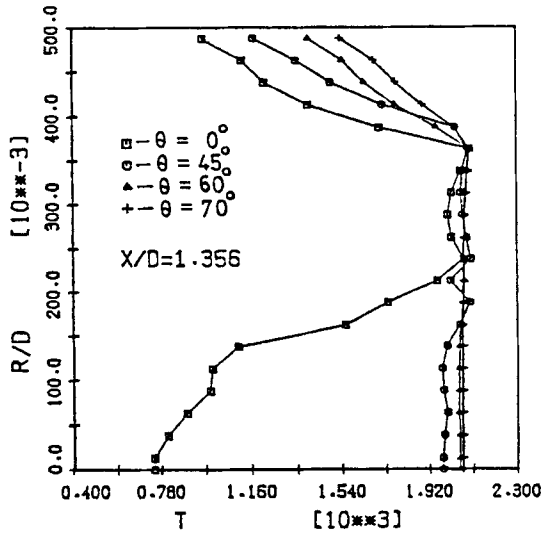

Figure 20. Temperature distribution at $X/D = 1{\cdot}356$ for various swirling angles (without flameholder)

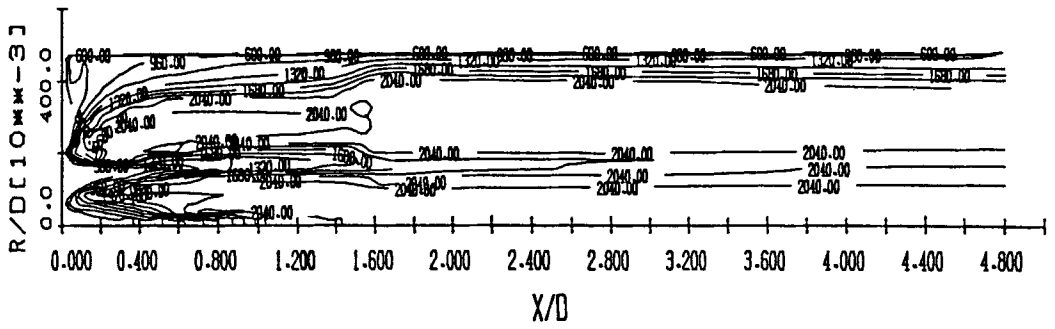

Figure 21. Temperature contours for case 1 ($\theta = 0°$)

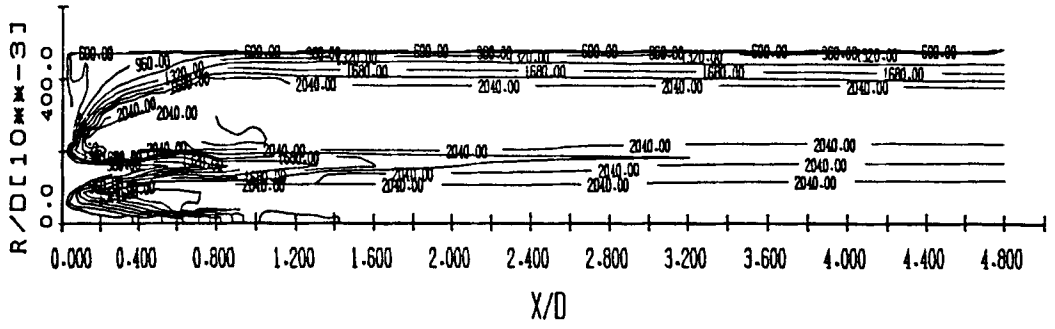

Figure 22. Temperature contours for case 2 ($\theta = 0°$)

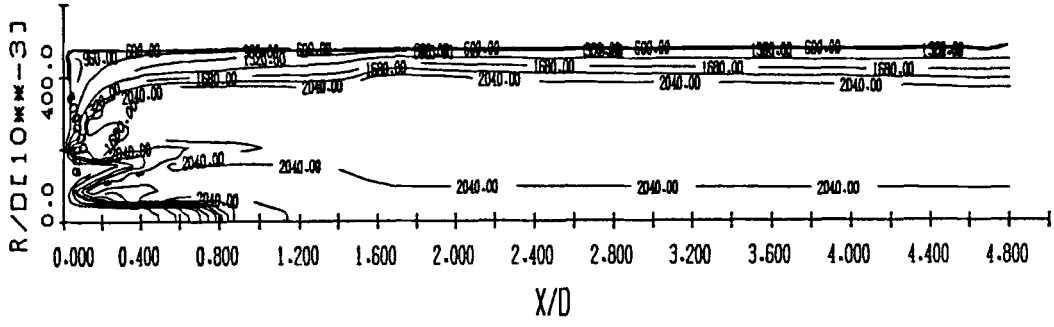

Figure 23. Temperature contours for case 1 ($\theta = 45°$)

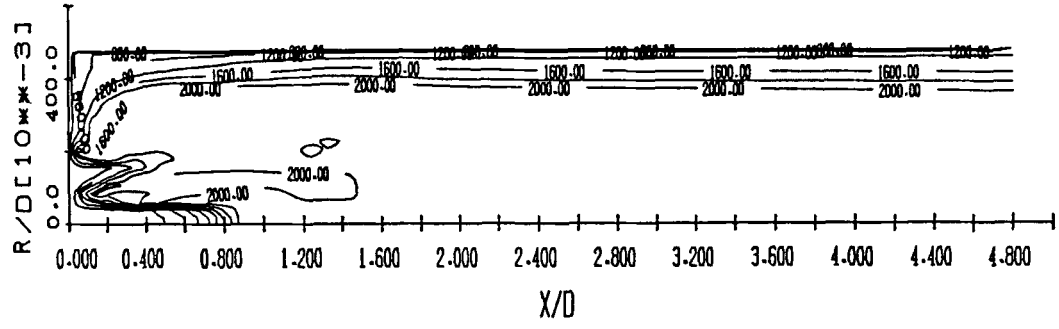

Figure 24. Temperature contours for case 2 ($\theta = 45°$)

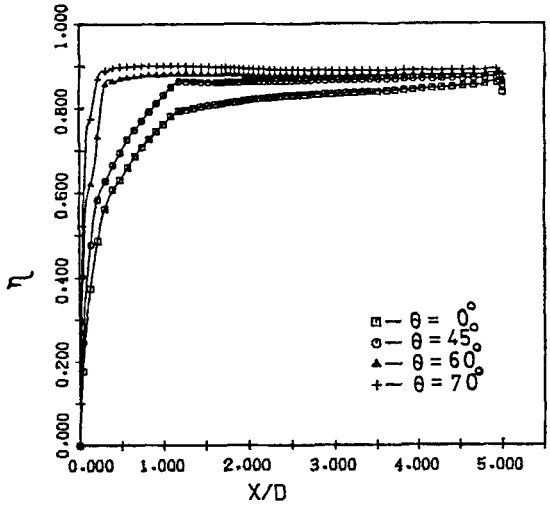

Figure 25. Combustion efficiency distribution of dump combustor (without flameholder)

temperature of the recirculation zone at the back of the flameholder is high owing to the recirculation effect. The temperature distributions for the flameholder of case 1 and case 2 at a swirling angle of $\theta = 45°$ are shown in Figures 23 and 24. For case 1 the temperature distribution at the back of the V-gutter is obviously not increased because the combustion process is already complete upstream of the flameholder. For case 2 the combustion process is not complete and the temperature is increased when the flameholder moves upstream.

High combustion efficiency is one objective of successful combustor design. The present combustion efficiency is defined as[37]

$$\eta = \frac{C_p(T_2 - T_1)_{\text{actual}}}{[(f/a)/(1+f/a)]\,\Delta H},$$

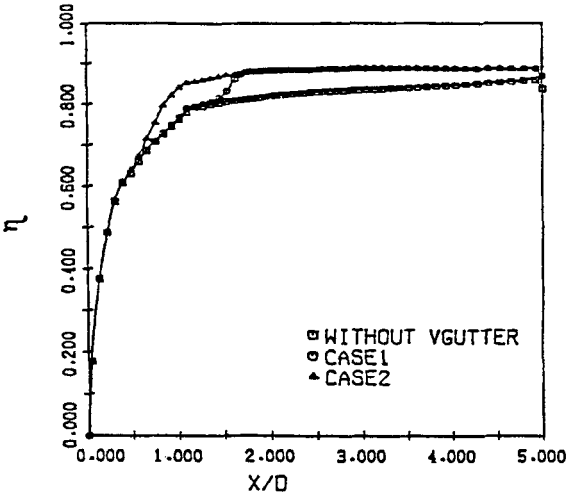

Figure 26. Combustion efficiency distribution ($\theta = 0°$)

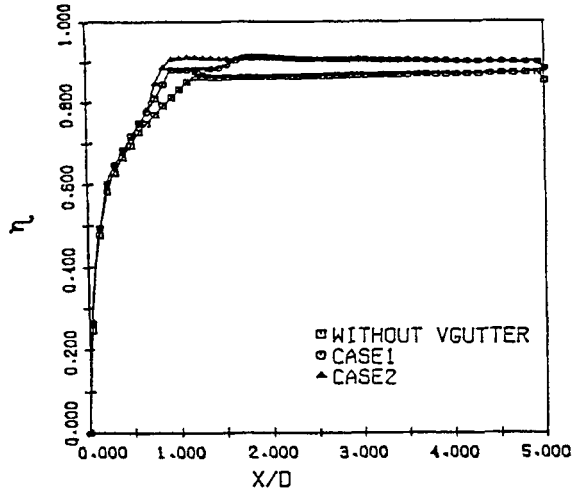

Figure 27. Combustion efficiency distribution ($\theta = 45°$)

where T_1 and T_2 are the inlet and exit temperatures respectively, C_p is the specific heat at constant pressure, f/a is the fuel–air mass ratio and ΔH is the heat of reaction per unit mass of fuel. The combustion efficiency of the dump combustor is increased when the swirling angle is increased, as shown in Figure 25. The combustion efficiency of the dump combustor at the back of the flameholder has been suddenly increased, as shown in Figures 26 and 27. This demonstrates that the flameholder effect has increased the combustion efficiency of the dump combustor. Also, the

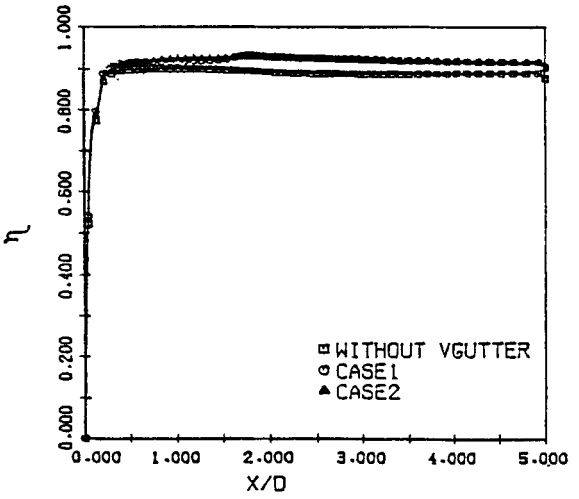

Figure 28. Combustion efficiency distribution ($\theta = 70°$)

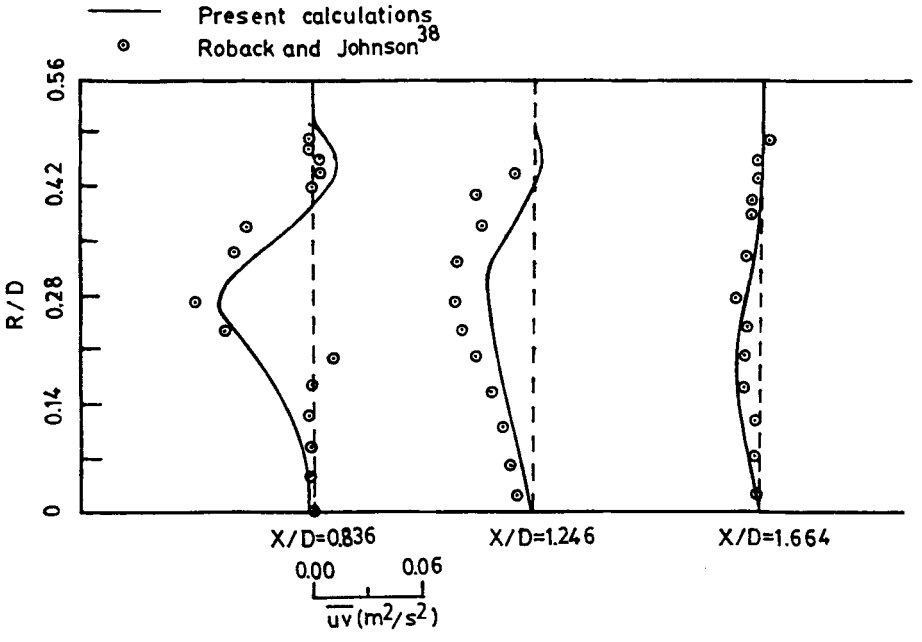

Figure 29. Axial–radial Reynolds stress distribution (ARS model, $\theta = 30°$)

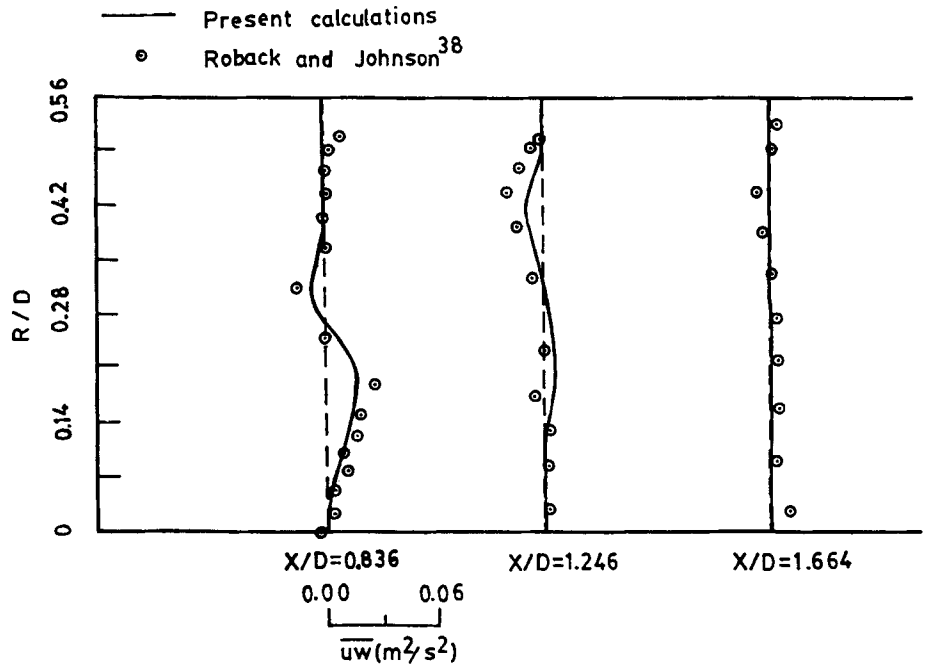

Figure 30. Axial–tangential Reynolds stress distribution (ARS model, $\theta = 30°$)

combustion efficiency of the dump combustor is increased when the flameholder moves upstream, as shown in Figures 25–27. The configuration effect of the flameholder on the combustion efficiency is not present when the swirling angle reaches 70°, as shown in Figure 28. Both the axial–radial and axial–tangential Reynolds stress distributions of the dump combustor at various cross-sections are shown in Figures 29 and 30. The qualitative analyses of the present calculations by the ARS model are in agreement with the experimental data of Roback and Johnson.[38] Agreement with the experimental Reynolds stress data is achieved by the algebraic Reynolds stress model (ARS model) based on the Reynolds stress equation, retaining its anisotropy, as shown in Figures 29 and 30.

CONCLUDING REMARKS

1. The turbulent kinetic energy is increased by means of the swirling effect.
2. The turbulent kinetic energy and turbulent mixing are promoted for the combustor with a flameholder.
3. The combustion efficiency of the combustor is increased for larger swirling angle.
4. The combustion process is complete, the temperature distribution is uniform and the combustion efficiency is increased for the combustor with a flameholder.
5. For $\theta \leqslant 45°$ the combustion efficiency of the combustor is increased when the configuration of the flameholder is moved towards the inlet region.
6. For $\theta \geqslant 60°$ the configuration effect of the flameholder on the combustion efficiency is not present.

7. The standard k–ε model is not satisfactory with strongly swirling flow, and although the Richardson number correction for the ε-equation can be used to give some improvement, it is still not adequate. The reason is that it predicts the eddy viscosity poorly. A further improvement can be made by using the algebraic Reynolds stress model for the present observations; because it shows a better prediction for the eddy viscosity, retaining its anisotropy.

APPENDIX: NOMENCLATURE

A_i	surface area of control volume
a_i	joint coefficient
b	residue mass
D	diameter of combustor
D_0	inlet diameter of combustor
F	total enthalpy
f	underrelaxation factor
ΔH	heat of reaction per unit mass of fuel
k	turbulent kinetic energy
L	length of combustor
m_{fo}	modified mass fraction
$m_{\mathrm{fu}}, m'_{\mathrm{fu}}$	mass fraction and reaction rate of fuel
$m_{\mathrm{ox}}, m'_{\mathrm{ox}}$	mass fraction and reaction rate of oxidant
P	static pressure
S^{ϕ}	source term of variable ϕ
$S_{\mathrm{p}}, S_{\mathrm{c}}$	coefficients of linearized source term
T	temperature
U, V, W	time-averaged velocity in directions x, r and θ
u, v, w	fluctuating velocity in directions x, r and θ
U_0	inlet velocity of combustor
ΔV	volume
x, r	co-ordinates in axial and radial directions

Greek letters

Γ_{ϕ}	transfer coefficient of variable ϕ
θ	inlet swirling angle
μ_{e}	effective viscosity
μ_{l}	molecular viscosity
μ_{t}	eddy viscosity
ε	dissipation rate of turbulent energy
ρ	density
ϕ	transport variable
ω	chemical reaction rate
η	combustion efficiency

Superscripts and subscripts

in	inlet property
nb	neighbourhood points

p, e, w, s, n	grid points
t	turbulent quantity
ϕ	physical variable

REFERENCES

1. D. G. Lilley, 'Primitive pressure–velocity code for the computation of strongly swirling flow', *AIAA J.*, **14,** 749–756 (1976).
2. C. C. Lu, 'Measurements of turbulent flow velocity for sudden expansion cylindrical tube using laser doppler velocimeter (LDV)', *AICHE J.* **26,** 303–305 (1980).
3. D. G. Lilley, 'Turbulent swirling flame prediction', *AIAA J.*, **12,** 219–223 (1974).
4. M. A. Leschziner and W. Rodi, 'Computation of strongly swirling axisymmetric free jets', *AIAA J.*, **22,** 1742–1747 (1984).
5. Z. C. Hong and H. C. Liao, 'Swirl effect on the structure of recirculation zone and fuel distribution of a coaxial dump combustor', *3rd Natl. Conf. on Mechanical Engineering* CSME, Chung-Li, 1986, pp. 323–344.
6. Z. C. Hong, J. L. Pan and C. Lin, 'Side dump combustor combustion analysis', *CSME J.*, **7,** 1–10 (1986).
7. G. H. Vatistas, S. Lin, C. K. Kwok and D. G. Lilley, 'Bluffbody flameholder wakes: a simple numerical solution', *AIAA Paper 82–1177*, 1982.
8. D. R. Kang, 'The flowfield and combustion analysis for the combustor with V-gutter flameholders', *Master Thesis*, Department of Mechanical Engineering, National Taiwan University, 1986.
9. S. H. Chuang and S. W. Lii, 'Combustion flowfield analysis of an afterburner with V-gutter flameholders', *Trans. AASRC*, **21,** 39–54 (1988).
10. J. E. Drewry, 'Fluid dynamic characterization of sudden expansion ramjet combustor flow fields', *AIAA Paper 77–203*, 1977.
11. L. H. Back and E. J. Roschke, 'Shear-layer flow regimes and wave instabilities and reattachment lengths downstream of an abrupt circular channel expansion', *J. Appl. Mech.*, **94,** 667–681 (1972).
12. E. E. Khalil, D. B. Spalding and L. H. Whitelaw, 'The calculation of local flow properties in two-dimensional furnaces', *Int. J. Heat and Mass Transfer*, **18,** 775–791 (1975).
13. D. G. Lilley 'Swirl flow in combustion: a review', *AIAA J.*, **15,** 1063–1078 (1977).
14. D. G. Lilley, D. L. Rhode and J. W. Samples, 'Prediction of swirling reacting flow in ramjet combustors', *AIAA Paper 81–1485* 1981.
15. S. H. Chuang and J. S. Jiang, 'Diffusion flame analysis of an afterburner as a function of the air–fuel ratio', *Int. j. numer. methods fluids*, **11,** 303–316 (1990).
16. S. H. Chuang and H. M. Sung, 'Numerical simulation of the dump combustor flow', *J. Eng., NCHU*, **1,** 57–72 (1990).
17. B. E. Launder, C. H. Pridden and B. I. Sharma, 'The calculation of turbulent boundary layers on spinning and curved surfaces', *ASME J. Fluids Eng.*, **99,** 231–239 (1977).
18. D. Lilley, 'Prediction of inert turbulent swirl flows', *AIAA J.*, **11,** 955–960 (1973).
19. S. W. Armfield and C. A. Fletcher, 'Comparison of k–ε and algebraic Reynolds stress models for swirling diffuser flow', *Int. j. numer. methods fluids*, **9,** 987–1009 (1989).
20. H. H. A. Al-Mohammed, Flow in turbulent coaxial free jets with and without recirculation, *Ph.D. Thesis*, University of London, 1978.
21. F. Boysan and J. Swithenbank, 'Numerical prediction of confined vortex flows', *Proc. Numerical Methods in Laminar and Turbulent Flow*, Venice, 1981; also *Report HIC 370*, Dept. of Chemical Engineering, University of Sheffield, UK., 1981.
22. F. Boysan, W. H. Ayers, J. Swithebank and Z. Pan, 'Three dimensional model of spray combustion in gas-turbine combustor', *J. Energy*, **6,** 368–375 (1981).
23. I. Kubo and F. C. Gouldin, 'Numerical calculations of turbulent swirling flow', *ASME J. Fluids Eng.*, **97,** 310–315 (1975).
24. W. Rodi, 'A new algebraic relation for calculating the Reynolds stresses', *ZAMM*, **56,** 219–221 (1976).
25. B. E. Launder and A. P. Morse, *Turbulent Shear Flows, Vol. 1*, Springer, Berlin 1979.
26. M. M. Gibson and B. A. Younis, 'Calculation of swirling jets with a Reynolds stress closure', *Phys. Fluids*, **29,** 38–48 (1986).
27. J. Rotta, 'Statistische Theorie Nichtomogener Turbulenz', *Z. Phys.*, **129,** 547–572 (1951).
28. K. Hanjalic and B. E. Launder, 'A Reynolds stress model of turbulence and its application to thin shear flows', *J. Fluid Mech.*, **52,** 609–638 (1972).
29. D. Naot, A. Shavit and M. Wolfshtein, 'Interactions between components of the turbulent velocity correlation tensor due to pressure fluctuations', *Isr. J. Technol.*, **8,** 259–269 (1970).
30. W. Rodi, The prediction of free turbulent boundary layers by use of a two-equation model of turbulence, *Ph.d. Thesis*, University of London, 1972.
31. D. G. Lilley, 'Investigations of flow fields found in typical combustor geometries', *NASA CR-3869*, 1985.
32. B. I. Sharma, The behavior of swirling turbulent boundary layers near walls, *Ph.D. Thesis*, University of London, 1975.

33. B. E. Launder and D. B. Spalding, *Lectures in Mathematical Models of Turbulence*, Academic, London, 1972.
34. D. G. Lilley and D. L. Rhode, 'A computer code for swirling turbulent axisymmetric reacting flow in practical isothermal combustor geometries', *NASA*-3442, 1982.
35. B. E. Launder and D. B. Spalding, 'The numerical computation of turbulent flows', *Comput. Methods Appl. Mech. Eng.*, **3**, 269–289 (1974).
36. M. C. Chaturvedi, 'Flow characteristics of axisymmetric expansion', *J. Hydraul. Div. Proc., ASCE*, **89**, 61–92 (1963).
37. G. C. Oates, 'The aerothermodynamics of aircraft gas turbine engines', *AFAPL TR78-52*, 1978.
38. R. Roback and B. V. Johnson, 'Mass and momentum turbulent transport experiments with confined swirling coaxial jets', *NASA CR-168252*, 1983.